Science of the Total Environment 657 (2019) 325–339

Contents lists available at ScienceDirect

Science of the Total Environment

journal homepage: www.elsevier.com/locate/scitotenv

Contributions of climate change and vegetation greening to evapotranspiration trend in a typical hilly-gully basin on the Loess Plateau, China

Meng Bai [a,b], Xingguo Mo [a,c,*], Suxia Liu [a,c], Shi Hu [a]

[a] Key Laboratory of Water Cycle and Related Land Surface Processes, Institute of Geographic Sciences and Natural Resources Research, Chinese Academy of Sciences, Beijing 100101, China
[b] University of Chinese Academy of Sciences, Beijing 100049, China
[c] College of Resources and Environment, Sino-Danish Center, University of Chinese Academy of Sciences, Beijing 100049, China

HIGHLIGHTS

- Land use/cover changes caused by GFG greatly affected the reginal water and energy balance.
- Simulation of ET_a layout in YRB using VIP model showed a clear increase trend.
- >90% of the ET_a trend can be explained by vegetation greening.
- Vegetation greening was mainly driven by GFG and <10% caused by climate change.

GRAPHICAL ABSTRACT

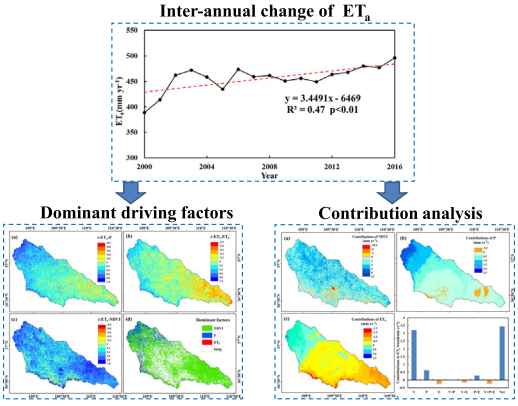

ARTICLE INFO

Article history:
Received 12 June 2018
Received in revised form 23 November 2018
Accepted 24 November 2018
Available online 27 November 2018

Editor: Ralf Ludwig

Keywords:
Evapotranspiration
NDVI
Contribution
VIP model
Partial correlation analysis
Loess Plateau

ABSTRACT

Significant increases in vegetation cover on the Loess Plateau since the early 2000s have been well documented. However, the relevant hydrological effects are still unclear. Here, we investigated the changes in actual evapotranspiration (ET_a) from 2000 to 2016 and related them to climate change and vegetation greening in Yanhe River basin (YRB), a typical hilly-gully basin on the Loess Plateau, by using the remote-sensing based VIP model. Results showed that the annual ET_a in the YRB increased significantly with a trend of 3.45 mm yr^{-1} ($p < 0.01$) and changes of ET_a in summer months dominated the annual trend. Partial correlation analysis suggested that vegetation greening was the dominant driving factor of ET_a inter-annual variations in 56% area of YRB. Model simulation experiments illustrated that relative contributions of NDVI, precipitation, and potential evapotranspiration (ET_p) to the ET_a trend were 93.0%, 18.1%, and −7.4%, respectively. Vegetation greening, which is closely related to the Grain for Green (GFG) afforestation, was the main driver to the long-term tendency of water consumption in the YRB. This study highlights potential water demanding conflicts between the socio-economic system and the natural ecosystem on the Loess Plateau due to the rapid vegetation expansion in this water-limited area.

* Corresponding author at: 11A, Datun Road, Chaoyang District, Beijing 100101, China.
E-mail address: moxg@igsnrr.ac.cn (X. Mo).

https://doi.org/10.1016/j.scitotenv.2018.11.360
0048-9697/

1. Introduction

Evapotranspiration (ET) plays a vital role in connecting water, energy, and carbon cycles in the terrestrial ecosystem (Zhang et al., 2015a). Due to climatic change and land use/cover changes, terrestrial ET process has been noticeably shifted on multiple spatiotemporal scales (Douville et al., 2013), which influences regional water cycle, vegetation growth, and feedback on the climate change, especially in arid and semiarid regions (Fisher et al., 2011). In addition, the long term tendency of ET has been regarded as a significant indicator of intensification of the regional water cycle (Mo et al., 2017). Therefore, a comprehensive understanding of the interactive roles of climate change and land use changes on spatial-temporal ET patterns is crucial for water resources management, ecosystem conservation, and adaption strategies to climate change.

The Loess Plateau is located in the middle Yellow River of China (Fig. 1) and is a typical arid and semi-arid area, where 85% of precipitation is consumed by ET (Feng et al., 2016). Since the kicking of Grain for Green Project (GFG) in 1999, the Loess Plateau has experienced substantial land use/cover changes, which are mainly characterized by large-scale conversion from cropland or sparse vegetation to grassland and shrub land habitat (Wohlfart et al., 2016). From 1999 to 2010, GFG has converted 16,000 km^2 of rain-fed farmland into forest or grassland (Feng et al., 2016). The NDVI trend of the Loess Plateau after 2000 is much faster than that before 2000 (Cao et al., 2018), and twice faster than that of the North China Plain during the same period (Chen et al., 2017). As a result, vegetation coverage on the Loess Plateau in the past two decades has significantly improved (Li et al., 2017b), increasing from 31.6% in 1999 to 59.6% in 2013 (Chen et al., 2015). In this period, climate change is detected, showing warming and drying trends before late 1990s and wetting and weakly cooling trends after this time (Li et al., 2015). Consequently, the Plateau ecosystems are significantly affected by climate change and human activities (Feng et al., 2013; Hou et al., 2017) whose direct or indirect effects on hydrologic cycles at multiple spatial and temporal scales are still unclear(Feng et al., 2016; Jiao et al., 2016; Li et al., 2016a).

Land use/cover change influences the ET process by altering surface roughness, albedo, and interception (Shen et al., 2015). Long-term changes in climate variables are also important driving factors for inter-annual tendency of ET (Xie et al., 2015; Yao et al., 2014; Mo et al., 2015). Most of the early studies on vegetation change-related ET responses were based on field experiments, which quantify effects of vegetation and climate changes on ET by comparing site-scale observed ET under different vegetation coverage or/and different climate conditions (Sun et al., 2008; Wang et al., 2008). Field experiment approach is very important to reveal the mechanisms of soil-vegetation-atmosphere interaction. However, they are generally constrained to field scale and the conclusions are usually inconsistent to those in other areas due to limitation on specific climatic conditions, soil types, and vegetation types.

Therefore, many researchers have used physically-based hydrologic models to reveal the effects of climate and land use changes on ET, runoff, soil water, and ground water under various scenarios(Li et al., 2009; Qiu et al., 2017; Tian et al., 2017; Li et al., 2016c; Yin et al., 2017). Such hydrological models are useful for estimating the hydrologic responses in basins or regions under various climate and land surface conditions, but they are usually characterized by complicated model structures, a lot of parameters, time consuming and uncertainty in model calibration and validation (Gao et al., 2016). In addition, some empirical models based on water balance or Budyko framework were also used to assess effects of climate and underlying surface changes on hydrological processes (Ning et al., 2017; Liang et al., 2015; Gao et al., 2017; Huang et al., 2016; Wang et al., 2015; Sun et al., 2006). These empirical models avoid uncertainties existed in the physically-based models and therefore provide a simple and effective method for attribution analysis (Roderick and Farquhar, 2011; Wang and Hejazi, 2011; Yang and Yang, 2011). However, they are generally considered to be incapable of obtaining temporal-spatial distribution of ET as they are mainly applicable to studies on the basin scale and annual scale.

Many field experiments studies indicated that responses and mechanisms of ET to changes of vegetation vary with vegetation type and composition (Gong et al., 2017; Sun et al., 2008). Moreover, the responses may change with spatial scale (Liu et al., 2016). The response mechanisms depending on the vegetation type and spatial scale cannot be completely reflected using traditional field experiments or empirical model approaches. As the advance of satellite, remote sensing provides broad spatial coverage and high temporal-spatial resolution of land surface characteristics and vegetation dynamics (Zhang et al., 2016). Hence, more and more studies are addressing the impacts of vegetation coverage change on ET process using remote-sensing based ET models or remote-sensing retrievals. For example, based on the satellite-estimated ET data sets, Feng et al. (2016) evaluated effects of

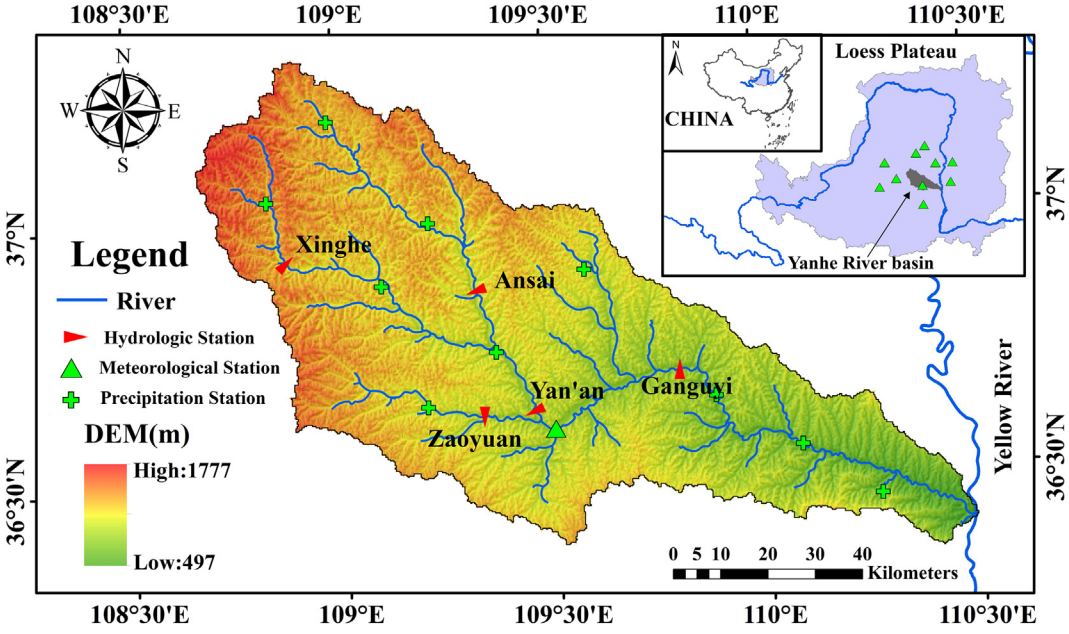

Fig. 1. Location of the Yanhe River basin.

revegetation program on the ecological environment and water resources of the Loess Plateau; Li et al. (2017a) investigated effects of land use and climate change on ET in China during 2001–2013.

Previous studies showed that with increasing vegetation coverage over the Loess Plateau, regional ET demonstrated obvious changes (Jin et al., 2017). In addition, interaction between vegetation growth and climate change has raised the complexities to understanding and quantification of the spatial-temporal ET patterns and their drivers. However, many studies only analyzed effects of climate change and vegetation greening on ET, and effects of climatic variations on vegetation growth were easily ignored. Therefore, contributions of human activities to the ET change may be overestimated. Furthermore, many remote-sensing based researches mainly investigated the ET response to the vegetation restoration, but few studies focus on the historical ET process and mechanisms that control ET dynamics, although better understanding of the ET evolution mechanism is crucial for predicting land surface-atmosphere interactions and terrestrial ecosystems in response to climate change and land-cover changes (Patle and Singh, 2015; Pei et al., 2017; Bai et al., 2018a).

In this study, the remote-sensing based and simplified Vegetation Interfaces Processes (VIP) model, which incorporates vegetation index into retrieving of vegetation dynamics and land surface characteristics, was used to simulate the ET temporal-spatial pattern from 2000 to 2016 in a typical basin of the Loess Plateau-Yanhe River basin (YRB). As one of the core areas of GFG program, YRB was selected for analyzing the hydrological responses to climate change and vegetation greening on the Loess Plateau. On the basis of simulated results, this study aims (1) to analyze the ET evolution process and mechanism; (2) to identify the dominant driving factor that control the inter-annual variations of ET; (3) to quantitatively differentiate the contributions of climate and vegetation changes to ET trend.

2. Method and materials

2.1. Study basin

Yanhe River basin (YRB), located in the middle part of the Loess Plateau, China (36°21′N–37°29′N, 108°38′E–110°29′E), covers an area of 7725 km^2 and is a typically hilly-gully region (Fig. 1). The average altitude and gradient of YRB are 1216 m and 17°, respectively. The altitude ranges from 497 m to 1777 m, decreasing gradually from the northwest to the southeast. Characterized by the typical warm temperate continental monsoonal climate, YRB has an annual mean temperature ranging from 8.8 °C to 10.2 °C. The multi-year average annual precipitation of YRB is 495 mm, wherein, over 70% of the precipitation falls from June to September. Yanhe River, with a length of 284.3 km, is a 1-class tributary of Yellow River. The mean annual runoff at Ganguyi, the most downstream hydrological station, was 199 million m^3 from 1980 to 2015. Runoff depth of YRB decreases from upstream to downstream, ranging from >45 mm to < 30 mm. The dominant land use types of YRB are forestland in the southern part, crop and grassland in the middle-southeastern part, and grassland in the northwestern part, respectively.

2.2. Model and data

2.2.1. Model introduction

Vegetation Interfaces Processes (VIP) model is a distributed eco-hydrological model developed originally at a point scale (Mo and Liu, 2001) and later extended to a catchment and regional scale (Mo et al., 2004; Mo et al., 2005) to simulate the exchanges of energy, water and carbon between land surface and atmosphere. For a quick, simplified and more convenient simulation to ET, the remote-sensing based VIP model was developed (Mo et al., 2015). The advantage of the remote-sensing based VIP model over other remote-sensing based ET models is its capability of long-term simulation to acquire the inter-annual and decadal feature of ET based on detail physical mechanism of the exchanges of energy, water and carbon between land surface and atmosphere adapted from the original VIP model. The details of the remote-sensing based VIP model can be found in Mo et al. (2015) and the Appendix A.

2.2.2. Data

The MODIS Land Cover Type product (MCD12Q1), which contains five types of classification systems, has an immeasurable significance in Earth surface research and has been widely used for different applications. Within the five types of classification systems, the Land Cover Type 1, based on the International Geosphere-Biosphere Programme (IGBP) classification, was used in this study.

The MODIS-NDVI dataset (MOD13Q1), spanning from 2000 to 2016 with 16-day temporal composite at 250 m spatial resolution, were used to retrieve vegetation dynamics and land surface characteristics. In this study, NDVI data with poor quality were firstly identified by interpreting the pixel reliability layer which marks pixels affected by cloud or ice/snow and provides a reliability index for each pixel. Then, the Savitzky-Golay (S-G) filter was applied to the original NDVI time series and the unreliable values were replaced by the reconstructed NDVI data. Reconstructing methods based on pixel reliability and S-G filter can yield more reliable NDVI time series (Chen et al., 2004). Take the NDVI data in day 225 as an example, the number of unreliable pixels was 27; NDVI data in these pixels were all corrected after the S-G filter was conducted, and the relative changes of NDVI values were basically below 30%. In order to match with the temporal scale in this model, the 16-day NDVI data were interpolated to daily values using the Lagrange polynomial method. In addition, the 8-km semi-monthly AVHRR GIMMS-3g NDVI data from 1981 to 2013 were used to investigate the vegetation condition of YRB before 2000.

Meteorological data, including daily precipitation, air temperature, air pressure, relative humidity, wind speed, and sunshine duration during 2000–2016, were obtained from China Meteorological Administration (CMA) at 10 stations inside and around the YRB. Additionally, daily precipitation data from 2000 to 2016 at 10 gauging sites inside the YRB were collected from the Hydrologic Yearbook of China. These data were gridded with the spatial resolution of 250 m by gradient inverse distance square (GIDS) method (Nalder and Wein, 1998). In-situ soil moisture data of Yan'an agrometeorological station (109°30′09.0″E, 36°36′14.0″N) are available in YRB. The relative soil water content (SWC) at the depth of 10 cm, 20 cm, 50 cm, 70 cm and 100 cm were measured every ten days from 2000 to 2013. These data were also obtained from the CMA and used to evaluate the performance of soil moisture simulations.

Eddy covariance flux measurements at wetland site (100°26′47.0″E, 38°58′30.5″N) (2014), farmland site (100°22′20.0″E, 38°51′19.8″N) (2013), and mixed forest site (101°08′0.6″E, 41°59′25.1″N) (2015) were used for model calibration. They were provided by "Heihe Plan Science Data Center, National Natural Science Foundation of China" (http://www.heihedata.org) (Liu et al., 2011; Xu et al., 2013b). The half-hour data were linearly interpolated. To control data quality, if data gaps in one day were >6 h, data on that day was rejected. Besides, monthly runoff data of 5 hydrological stations (Fig. 1) in YRB were collected from the Hydrologic Yearbook of China. They were used to estimate the domain average actual ET (ET_a) at monthly or annual scale based on basin-scale water balance equation.

The Gravity Recovery and Climate Experiment (GRACE) data provide an opportunity to constrain hydrological model parameterizations in combination with streamflow observations (Bai et al., 2018b). In this study, GRACE RL05 data during 2003–2015 released by Center for Space Research of University of Texas (CSR) were used for validation of modeled monthly ET_a (https://grace.jpl.nasa.gov/data/get-data/monthly-mass-grids-land/). The GRACE satellite acquires monthly terrestrial water storage anomalies (TWSA) by monitoring changes of earth gravitational field. In the GRACE RL05 data, effects of the atmosphere, oceans, and tides were removed. Therefore, they mainly reflect

changes of terrestrial water storage (TWSC), including changes of surface water, soil water, and ground water storage (Tapley et al., 2004). The GRACE RL05 data had been corrected by the CSR using de-striping filter and Gaussian filter to minimize effects of correlated errors and algorithm errors. In this study, the data were re-corrected by scaling factor approach to restore signal losses arising from the sampling and post-processing of GRACE data (Landerer and Swenson, 2012). The missing data were filled up using cubic Lagrange interpolation. Monthly ET_a can be expressed as a residual of water balance equation in this basin:

$$ET_a = \mathrm{P}-\mathrm{R}-\mathrm{ds}/\mathrm{dt} \quad (1)$$

where P and R represent monthly precipitation and monthly runoff, respectively; ds/dt is the time derivative of TWSA. The central difference of monthly TWSA was used to approximate ds/dt.

2.3. Methodology

Evapotranspiration (ET) was simulated by the remote-sensing based VIP model (Mo et al., 2015). Trends of ET, NDVI, and climate variables were determined by the slope of the simple linear regression model. Relationships between ET, NDVI, and climate variables were quantified by calculating correlation coefficients between variables. All correlation analyses were done with the linear trends removed in order to focus on the relationship of year-to-year variations.

In order to identify the dominant driving factors that control inter-annual variations of ET_a, we conducted partial correlation analysis between ET_a and precipitation, potential ET (ET_p), and NDVI on the pixel scale, with all variables de-trended. For each grid cell, the variable that has the highest partial correlation coefficient is identified as the dominant driving factor. In order to eliminate influences of collinearity, we used regression analysis similar to the methods of Wang et al. (2017) to remove the effects of climate variables on actual NDVI before the partial correlation is conducted.

Eight simulation experiments (Table 1), based on the factor separation methodology proposed by Stein and Alpert (1993), were designed to quantitatively differentiate effects of climate change (precipitation and ET_p) and vegetation greening (NDVI) as well as their interactions on ET_a trend. In this methodology, interactive effects of predictor variables on response variable can be interpreted as the second-order or higher-order terms in Multi-point Taylor expansion. The simulation results of ET_a trend were represented by a general function, f. In each simulation experiment, one or more variables vary according to observation records while other variables vary according to control conditions (Zhang et al., 2015a). For example, $f(NDVI)$ represents simulation results when NDVI varies according to remote sensing observation records while all climatic variables are de-trended. The control simulation ($f(control)$) is the simulation results when all climatic variables are de-trended and NDVI is fixed at the year of 2000. The main effect of each variable on ET_a trend is represented by the difference between the simulation with only one varied variable and control simulation. For example, main effects of NDVI and P on ET_a trend are as follows:

$$E_{NDVI} = f(NDVI) - f(control) \quad (2)$$

$$E_P = f(P) - f(control) \quad (3)$$

where E_{NDVI} and E_P represent effects of NDVI and precipitation on ET_a trend, respectively.

The two-way interactive effect of variable A and B was calculated by subtracting the main effects of A and B from the effect of the joint A plus B. For example, the two-way interactive effect of NDVI and P is expressed as:

$$E_{NDVI\tilde{n}P} = f(NDVI, P) - f(control) - E_{NDVI} - E_P \quad (4)$$

The three-way interactive effect between *NDVI*, *P*, and ET_p was calculated by subtracting the three main effects and three two-way interactive effects from simulation results in real condition, namely:

$$E_{NDVI\tilde{n}P\tilde{n}ET_p} = f(NDVI,P,ET_p) - f(control) - E_{NDVI\times P} - E_{NDVI\times ET_p} - E_{P\times ET_p} - E_{NDVI} - E_P - E_{ET_p} \quad (5)$$

In this study, control conditions of climatic variables are defined as de-trended values rather than multi-year mean values adopted in other researches, because climatic variables always act coordinately with each other and de-trended values preserve intra-annual variations of variables in different years.

Table 1
Summary of all simulation experiments conducted in this study.

No	Simulation experiment	Description
1	$f(control)$	NDVI is fixed at the year of 2000 and all climatic variables are de-trended.
2	$f(NDVI)$	NDVI varies according to remote sensing observation records; all climatic variables are de-trended.
3	$f(P)$	Precipitation varies according to observation records; NDVI and other climatic variables vary according to control conditions.
4	$f(ET_p)$	All climatic variables except precipitation vary according to observation records; precipitation and NDVI vary according to control conditions.
5	f(NDVI,P)	NDVI and precipitation vary according to observation records; other climatic variables vary according to control conditions.
6	$f(NDVI, ET_p)$	Precipitation is de-trended; NDVI and other climatic variables vary according to observation records.
7	$f(P, ET_p)$	All climatic variables vary according to observation records; NDVI is fixed at the year of 2000.
8	$f(NDVI, P, ET_p)$	NDVI and all climatic variables vary according to observation records.

3. Results and analysis

3.1. Model validation

Over the long-term period, comparisons between simulated and water balance-based annual mean ET_a for 5 sub-basins in YRB from 2000 to 2016 indicated that this model generally performed well because it captured the general spatial pattern of ET_a in YRB (Fig. 2). However, the mean bias between simulated and observed ET_a was -12.4 mm yr^{-1} and the RMSE was 28.7 mm yr^{-1}, indicating that the model slightly underestimated annual ET_a in YRB.

Fig. 3 illustrated comparisons between GRACE-derived and simulated spatially averaged ET_a on the monthly scale and on the annual scale. In order to reduce the uncertainty due to errors in GRACE data, a 3-month moving-average smoothing was applied to the monthly series. In general, intra-annual and inter-annual fluctuations of simulated and

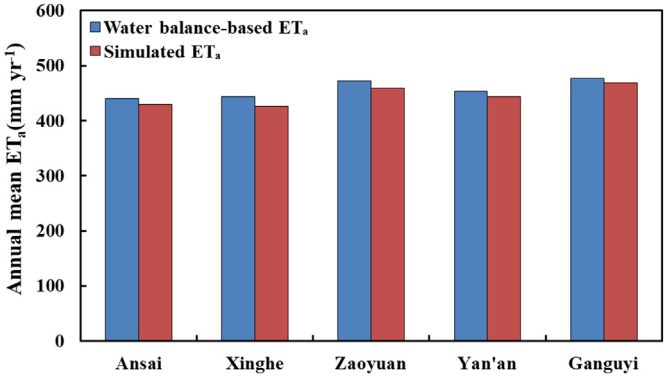

Fig. 2. Comparisons of simulated and water balance-based annual mean ET_a from 2000 to 2016 in 5 sub-basins of YRB. Yan'an and Ganguyi represent the catchment areas between this station and upstream station, respectively.

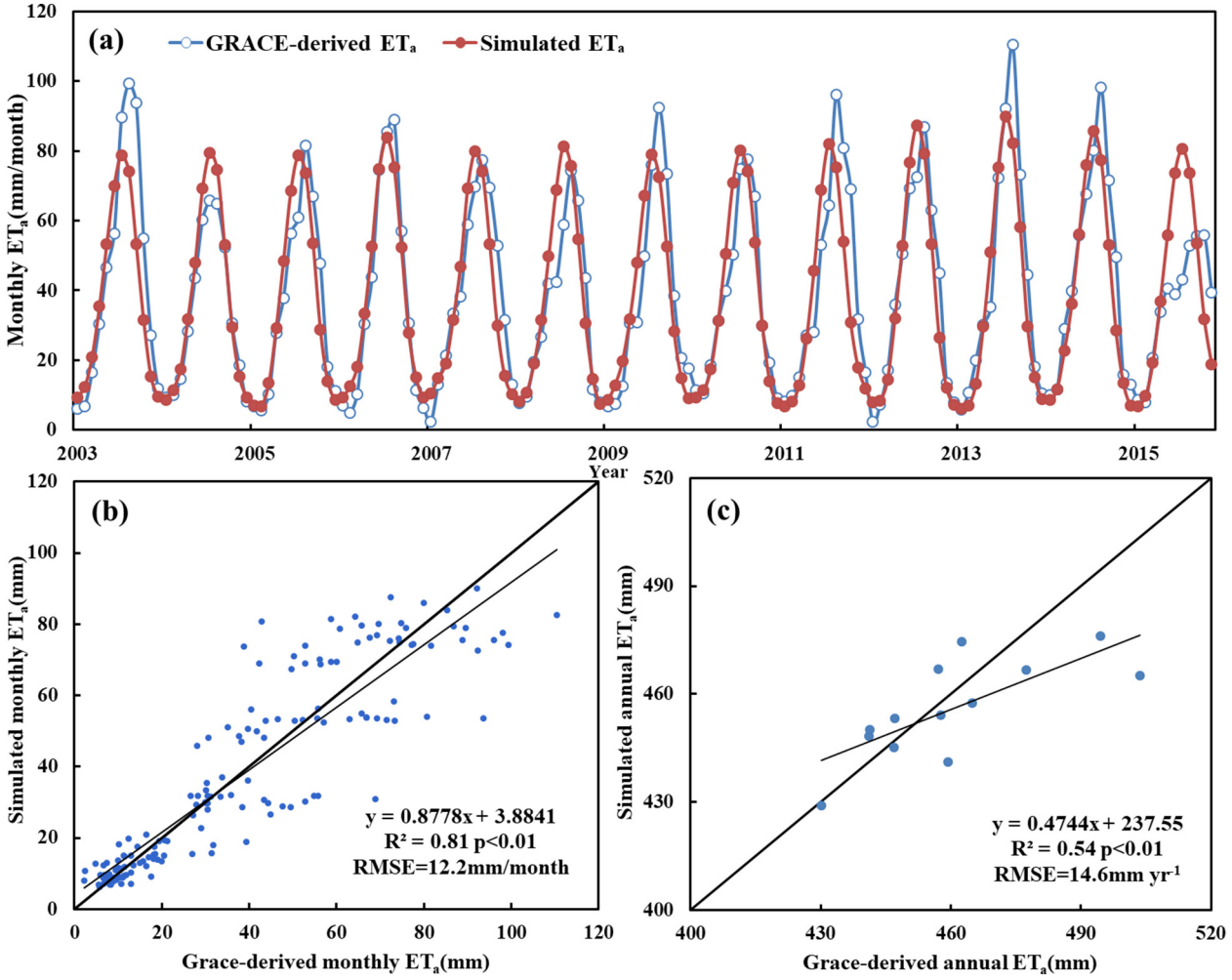

Fig. 3. Comparisons of simulated and GRACE-derived ET_a on the monthly scale (a, b) and on the annual scale (c). A 3-month moving-average smoothing was applied to the monthly series.

GRACE-based ET_a were basically consistent, exhibiting strong correlation ($R^2 = 0.81$ for monthly series and $R^2 = 0.54$ for annual series). However, GRACE-based monthly ET_a generally showed higher amplitude in summer than simulated ET_a. Averaged over the whole period, GRACE-based annual ET_a was 11.7 mm yr^{-1} higher than the simulated ET_a. A possible reason for this difference was that the impacts of check-dams and irrigation were not comprehensively considered in this model.

As for the SWC, there was some systematic deviation between simulated values and observations at Yan'an crop field site (Fig. 4). The simulated SWCs were generally higher than the observed especially when the storages were below 150 mm. However, the simulated SWCs basically traced the seasonal fluctuation of the field observations (Fig. 4a).

Three flux tower data were used to verify the model predictions in semi-arid to arid zone of Northwestern China. Averaged over the pixels around the test sites, the simulated daily ET_a were validated with

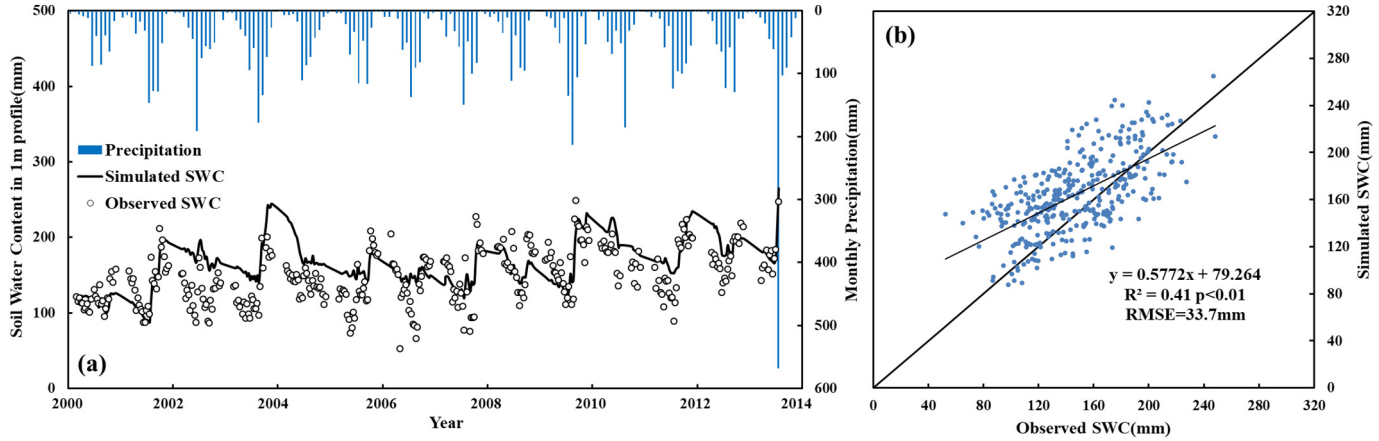

Fig. 4. Comparisons of the simulated and observed 10-day soil water content within 1 m profile at Yan'an crop field site from 2000 to 2013.

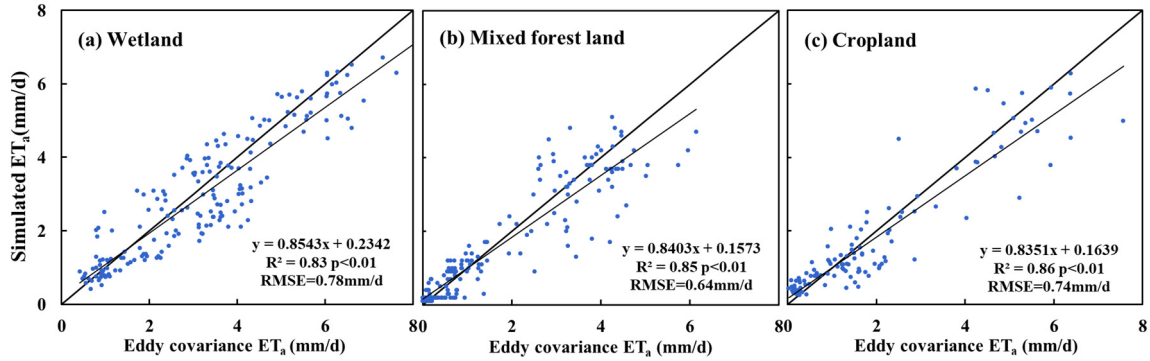

Fig. 5. Comparisons of the simulated daily ET_a with eddy covariance measurements.

measurements of eddy covariance at wetland, mixed forest and farmland sites (Fig. 5). The simulated and measured daily ET_a were significantly correlated with all coefficients of determination (R^2) being >0.82, and all root mean square errors (RMSE) being <0.80 mm/d at the three sites (Fig. 5(a–c)). The best fit lines were all around the 1:1 line. Therefore, the model performed fairly well in simulating ET_a both on the basin scale and on the site scale, indicating that it has a good potential for analyzing spatial-temporal pattern of ET_a in YRB.

3.2. Spatial patterns of ET, P, and NDVI

Under certain climate and vegetation conditions in a basin, long-term annual ET_a is principally controlled by both precipitation and available energy (represented by ET_p) (Budyko, 1974). As shown in Fig. 6(a), simulated annual ET_a exhibited large spatial variability, decreasing gradually from southeastern to northwestern areas and ranging from 324 to 549 mm. The spatial pattern of annual ET_a was basically consistent with that of annual precipitation (P) (Fig. 6(b)). Averaged over the whole basin, multi-year averaged ET_a was 457 ± 26 mm, which accounted for >90% of the corresponding precipitation. This fact indicated that most of the precipitation eventually returned to the atmosphere through evaporation and that changes in annual ET_a were mainly regulated by precipitation in decadal scale. Compared with precipitation, spatial pattern of annual ET_a was more consistent with that of NDVI ($r = 0.71$), indicating that vegetation patterns regulate the spatial change of annual ET_a. However, annual ET_a values in irrigated croplands were generally higher than that in surrounding natural vegetation areas.

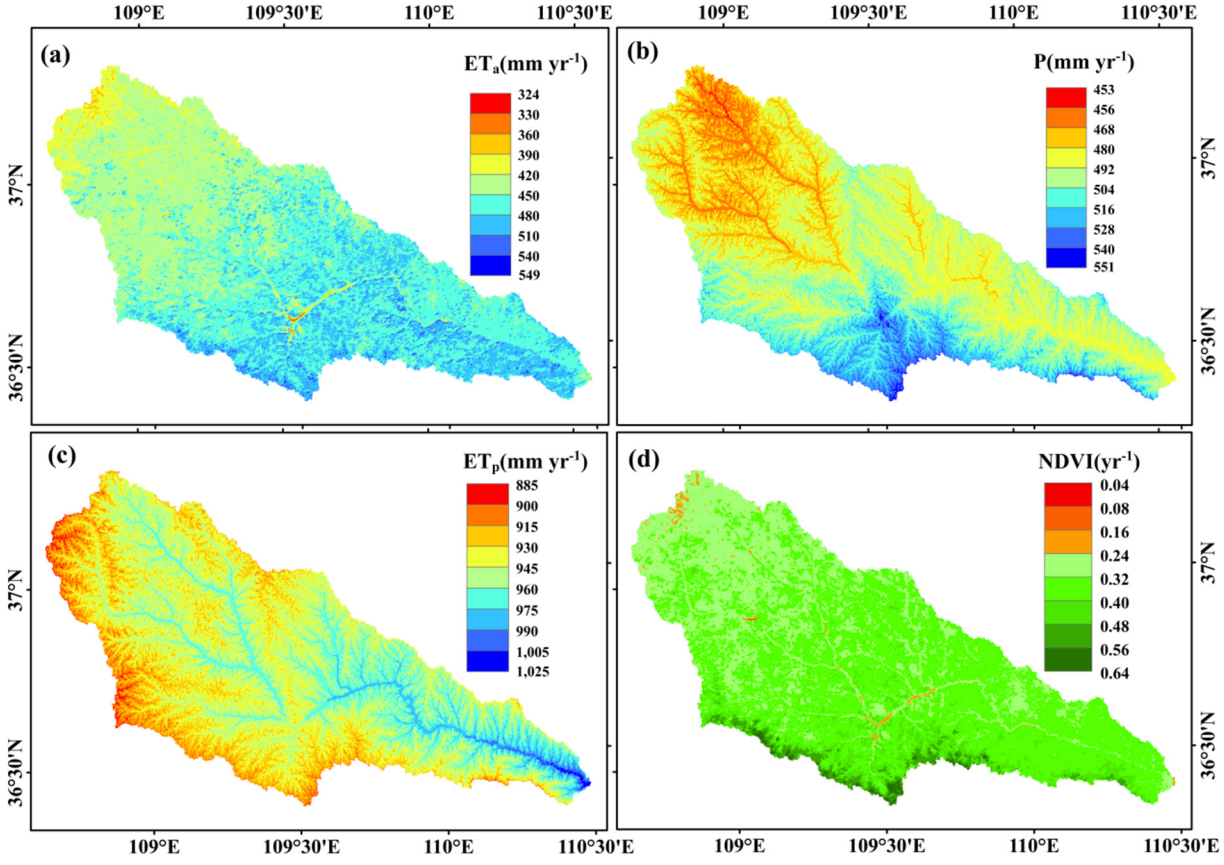

Fig. 6. Spatial patterns of mean annual (a) actual ET (ET_a), (b) precipitation (P), (c) potential ET (ET_p) and (d) NDVI over the period 2000–2016 in YRB.

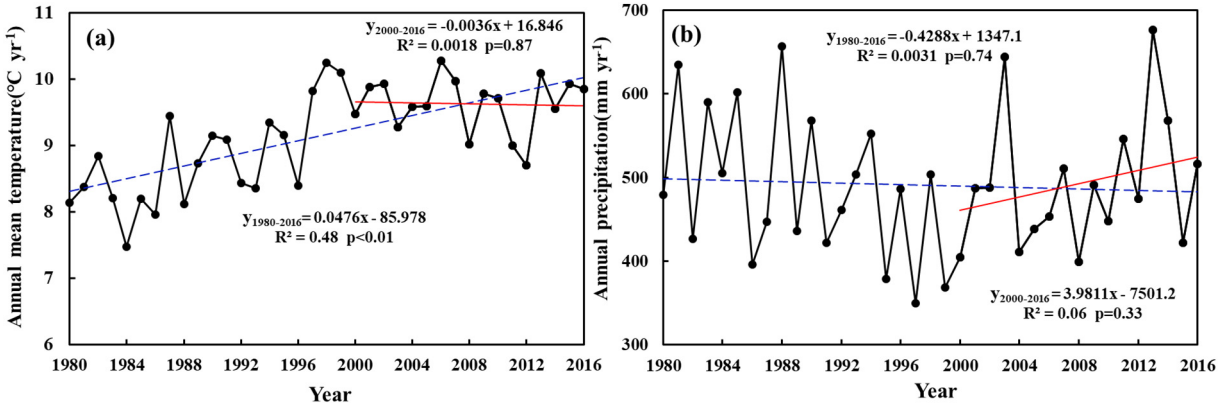

Fig. 7. Time series of annual mean temperature (a) and annual precipitation (b) of YRB from 1980 to 2016.

3.3. Spatial-temporal changes of climate, NDVI and ET

Climate change and human activities are the dominant driving forces of the evolution of regional eco-hydrological processes (Mo et al., 2017). Variations of climatic variables may exert remarkable impacts on vegetation water consumption. Human activities directly or indirectly affect growth of natural vegetation and crop through ecological restoration and agricultural management, which has a profound effect on the basin eco-hydrological processes.

3.3.1. Change in climate

During 1980–2016, climate of YRB showed a warming-drying trend on the whole, with the spatially averaged trends of 0.48 °C per decade for air temperature and −4.3 mm per decade for annual precipitation, respectively (Fig. 7). However, this warming-drying trend has slowed down since 2000, because air temperature rise tended to level off while precipitation even showed an increasing trend. On a monthly scale (Table 2), air temperature in spring (March and April) and autumn (from August to November) still showed an increasing trend, indicating that the growing season was still extending after 2000, which was beneficial to vegetation growth. In addition, monthly precipitation showed an increasing trend in spring months (from February to May), which provided favorable conditions for natural vegetation and crop growth in early period of the growing season.

3.3.2. Land use change and vegetation greening

Engineering measures of GFG includes conversion of farmland to forest/grassland, afforestation of barren land, and mountain closure for natural restoration. In YRB, large-scale land use changes mainly occurred in 1999 to 2004, when plenty of slope cropland was converted into artificial forestland or grassland and lots of barren land was afforested. Therefore, accumulative afforestation increased quickly in YRB before 2004 (Fig. 8a). After 2004, the focus of GFG gradually shifted to consolidation of existing achievements and gradual ecological restoration (Li et al., 2015) and more attention was paid to natural restoration of vegetation. Then, areas of mountain closure and afforested areas from barren land increased year by year. As a result, the ratio of forestland increased from 11.5% to 14.4% and that of cropland reduced from 43.1% to 40% from 2000 to 2015. The dominant land use change was transformation from cropland to forestland or from cropland to grassland (Fig. 8b).

GIMMS NDVI (1982–2013) and MODIS NDVI (2000–2016) were used to reveal historical vegetation changes in YRB. As shown in Fig. 9a, GIMMS NDVI did not exhibit significant rising before 1999, while it obviously increased after 2000. Similarly, MODIS NDVI also showed a significant increasing trend from 2000 to 2016 with an annual increase of 0.0094 yr^{-1} ($p < 0.01$). MODIS NDVI experienced a rapid increase from 2000 to 2002, and then a relatively slow but stable increasing trend from 2002 to 2016. On a monthly scale, MODIS NDVI increased significantly in all months (Fig. 9b). The most noticeable increases in NDVI occurred from May to July. The NDVI increases in these months were almost triple those in March and November.

Spatially, NDVI showed an increasing trend in almost the whole basin (99.4%) and areas with a significant trend accounted for 98.2% area of the YRB (Fig. 10a). In accordance with GFG implementation area, the spatial extent of significant increase in NDVI was mainly distributed in the central and northwestern areas of YRB. In urban areas, especially in new district of Yan'an City, NDVI significantly decreased due to urbanization.

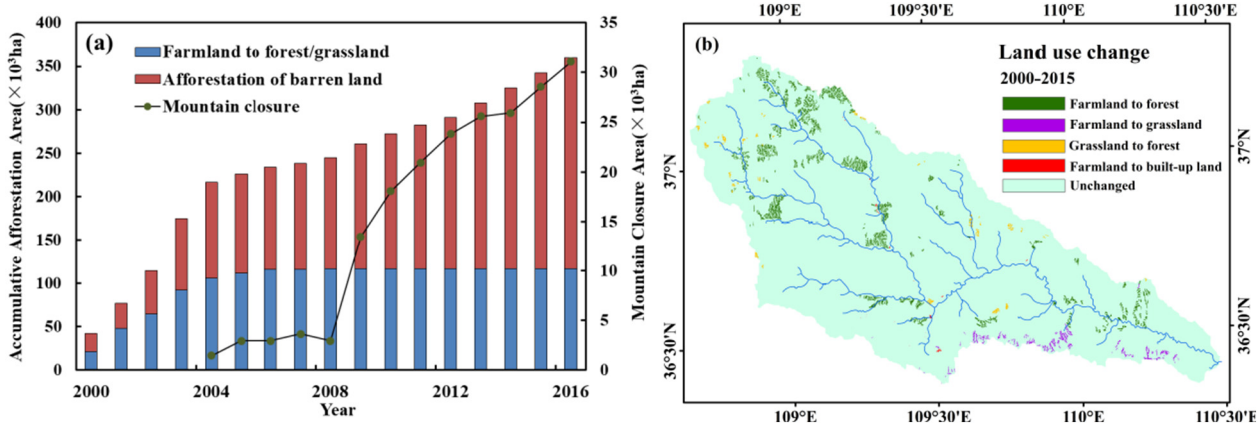

Fig. 8. Accumulative afforestation areas during 2000–2016 (a); land use change from 2000 to 2015 (b).

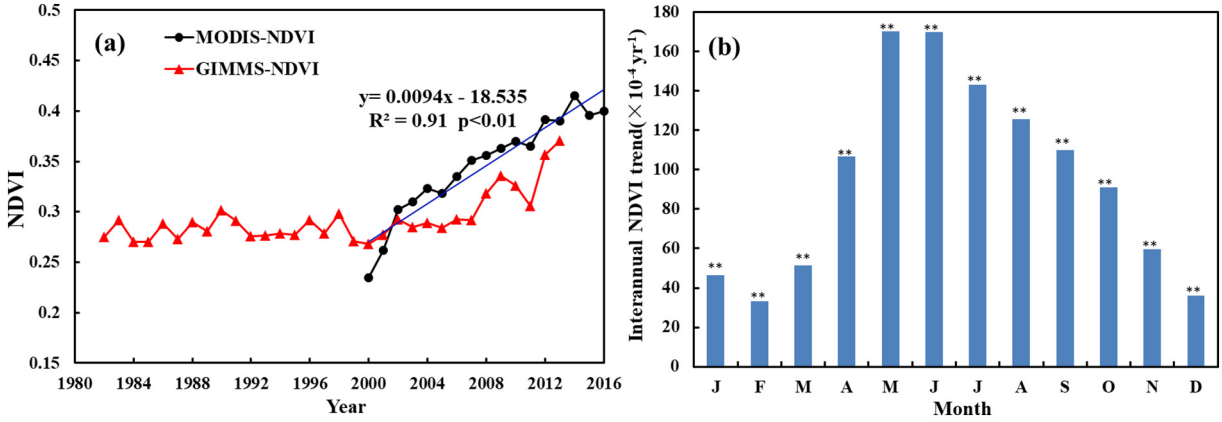

Fig. 9. Spatial average trends of NDVI at annual (a) and monthly (b) scales during 2000–2016 (significance levels: ** is $p < 0.01$).

3.3.3. Change in ET

From 2000 to 2016, annual potential ET (ET_p) showed an insignificant decreasing trend (Fig. 11a), resulted from the offsetting between the negative effects of reduced sunshine duration and increasing relative humidity, and the positive effect of increasing wind speed. At the same time, ET_a showed a significant increasing trend ($p < 0.01$), being consistent with the enhancement of greenness. It is noticed that the inter-annual variations of ET_a and ET_p coincided with the complementary relationship. Over the whole basin, spatially averaged ET_a trend from 2000 to 2016 was 3.45 mm yr^{-1} with Cv of 0.06 (Fig. 11a). In general, ET_a experienced a rapid increase before 2002 and a relatively slow but steady increasing trend after 2002, which was basically consistent with the inter-annual evolutions of NDVI. This fact indicated that the long-term change of annual ET_a was mainly dominated by vegetation greening. However, the inter-annual variations of ET_a were also affected by other factors. For example, a rapid decline in ET_a from 2003 to 2005 was mainly affected by a sharp decline in precipitation (Fig. 7b), whereas a slight decline in ET_a from 2006 to 2011 may resulted from the relatively low precipitation and a significant decrease in ET_p. On a monthly scale, ET_a mainly increased in summer months (From May to Aug) (Fig. 11b). The main reason was that the largest increase in NDVI occurred in summer when ET_a was generally not limited by water and energy. However, an increasing trend of ET_a may cause potential water stress because no significant trend was detected in summer precipitation.

Spatially, ET_a increased in 94% area of the YRB and areas with a significant positive trend accounted for 64.7% area of the whole basin (Fig. 10b). The spatial pattern of ET_a trends was consistent with that of NDVI trends. The positive trends of ET_a in grasslands in the northwest were the largest, then those in farmland in the middle and southeast, and last those in forestland in the south. ET_a was significantly decreasing in the new developing area.

3.4. Dominant driving factors of ET_a inter-annual change

Despite the increase of annual ET_a over the study basin, annual ET_a showed high fluctuations (Fig. 11a). In order to identify the dominant driving factors which controlled the year-to-year change of ET_a, partial correlation analysis between ET_a and its driving factors (P, ET_p and NDVI) was performed for each grid over the YRB during 2000–2016. Partial correlation coefficients(r) between ET_a and NDVI had high spatial consistency (Fig. 12c), with 95.6% of pixels being positively correlated, and 62.3% of pixels being significant ($p < 0.1$). High r values were mainly distributed in the southeastern area with abundant precipitation; r values in the northwestern area with sparse vegetation were also quite high. The correlations between ET_a and P were generally positive (Fig. 12a), but statistically significant in only 25.2% of pixels ($p < 0.1$), which mainly located in the northwestern part with low precipitation. In the southeast of YRB, where farmland is dominant, irrigation alleviated water stress in dry years, so correlation between ET_a and precipitation was relatively weak and negative correlations were found in some areas. The spatial pattern of r values between ET_a and ET_p showed obvious spatial heterogeneity (Fig. 12b), with positive correlations mainly in the northwest and negative correlations mainly in the southeast (5.2% and 8.2% with significant level, $p < 0.1$).

Dominant driving factors of ET_a changes for each pixel were identified based on spatial distribution of partial correlation coefficients (Fig. 12d). The result showed that NDVI controlled the inter-annual

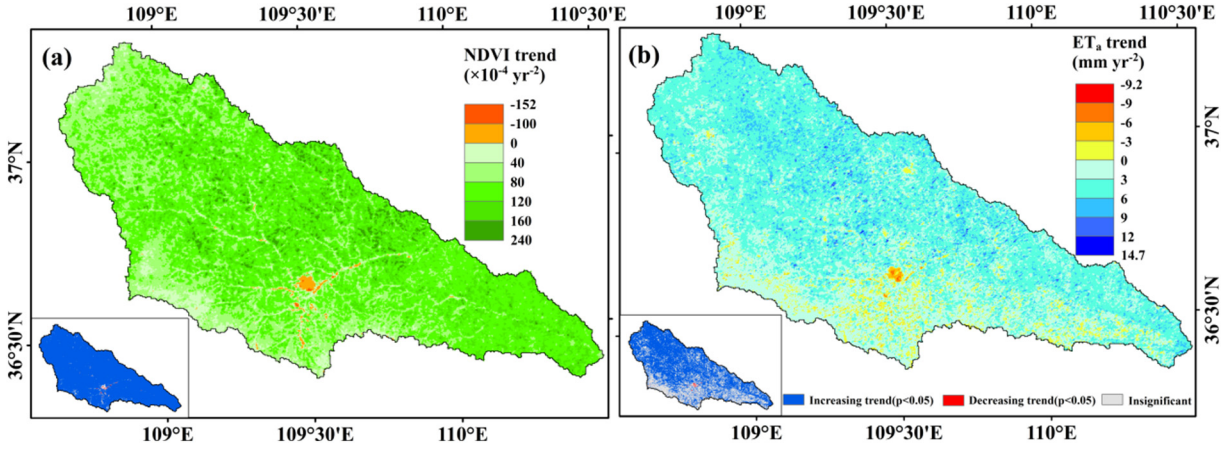

Fig. 10. Spatial patterns of annual trends of NDVI (a) and ET_a (b) in YRB during 2000–2016.

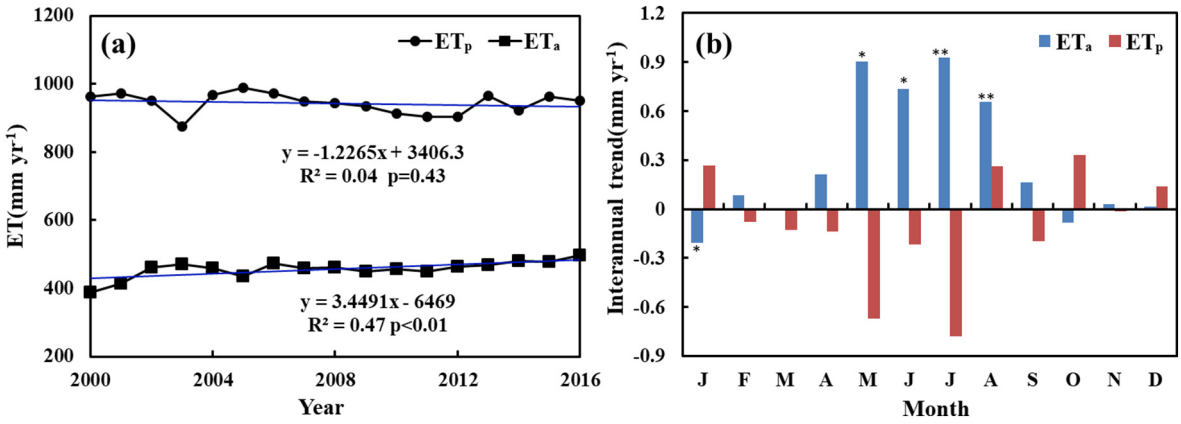

Fig. 11. Inter-annual trends of annual ET_a and ET_p (a) and trends of monthly ET_a and ET_p (b) from 2000 to 2016 (significance levels: ∗ is $p < 0.05$; ∗∗ is $p < 0.01$).

changes of ET_a in 56% of the YRB, while precipitation regulated the inter-annual changes of ET_a in 11.6% of the whole basin, mainly located in the northwest with low precipitation. ET_p played a dominant role in ET_a changes only in 0.5% of the study basin, which were scattered in forestlands in the southwest.

3.5. Contributions of climate change and vegetation greening to ET_a trend

Contributions of NDVI, precipitation, and ET_p to ET_a trend illustrated remarkable spatial heterogeneities (Fig. 13). Generally, the vegetation greening had a positive effect on ET_a trend (Fig. 13a). In the middle and northwestern parts of YRB, where vegetation greening was distinctive, the contributions of NDVI to the ET_a trend were relatively high with a value of >4 mm yr^{-2} and even >8 mm yr^{-2} in some areas. In the southern part, where forest is dominant and the greening trend was weak, the contributions of NDVI were relatively low with a value of <2 mm yr^{-2}. Vegetation degradation occurred in and around Yan'an city due to expansion of urban and dwelling buildings, leading to a sharp decline in ET_a. In the new district of Yan'an City, ET_a decreased most with a trend value of less than −6 mm yr^{-2}. The contributions of precipitation to ET_a trends were positive almost in the whole basin, ranging from −0.3 to 2.5 mm yr^{-2} and decreasing from the northwest to the southeast (Fig. 13b). Unlike NDVI and precipitation, ET_p change exerted a negative effect on ET_a trend in most parts of the YRB, with the contribution values ranging from −2.2 to 1.5 mm yr^{-2} (Fig. 13c).

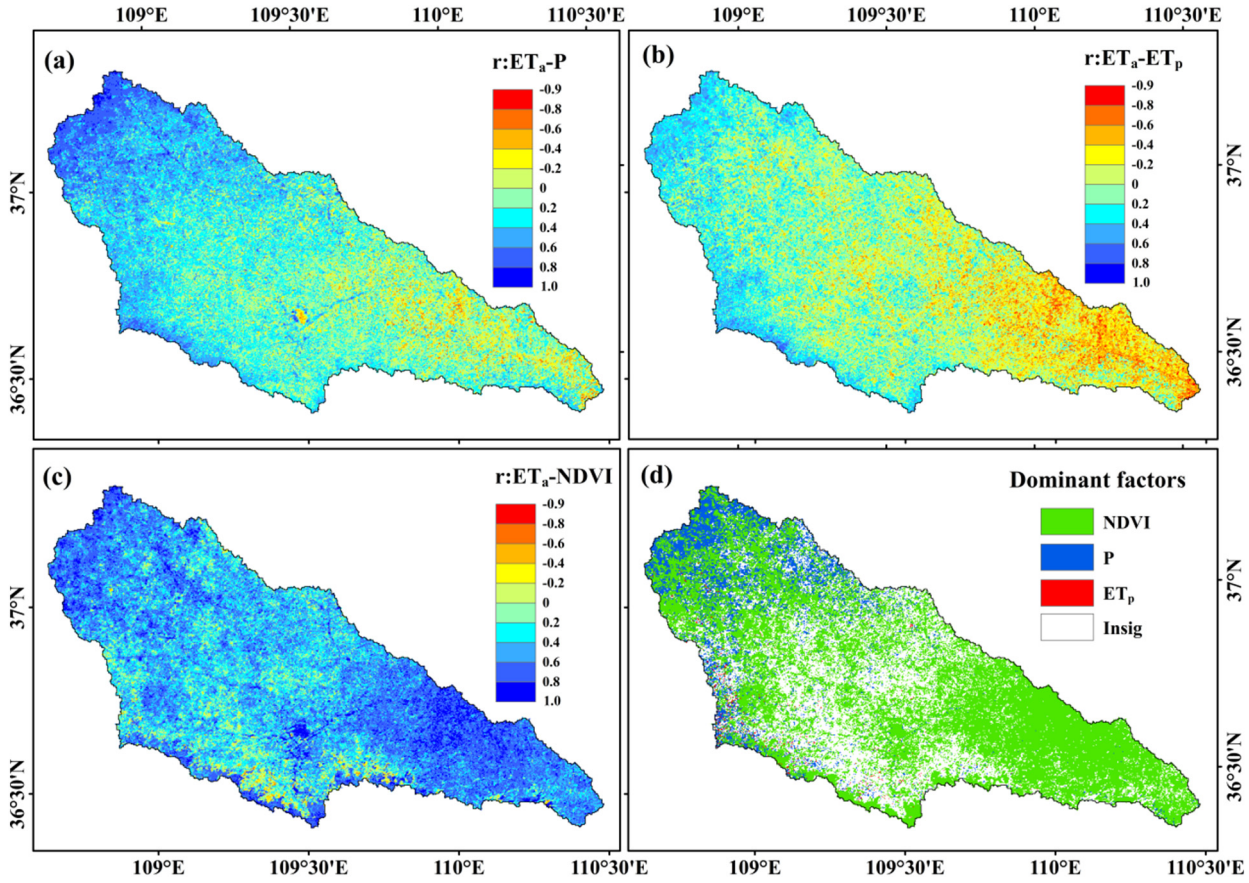

Fig. 12. Spatial patterns of partial correlation coefficient (r) between annual ET_a and (a) Precipitation(P), (b) ET_p and (c) NDVI; and (d) the dominant driving factors of the inter-annual change of ET_a in YRB from 2000 to 2016.

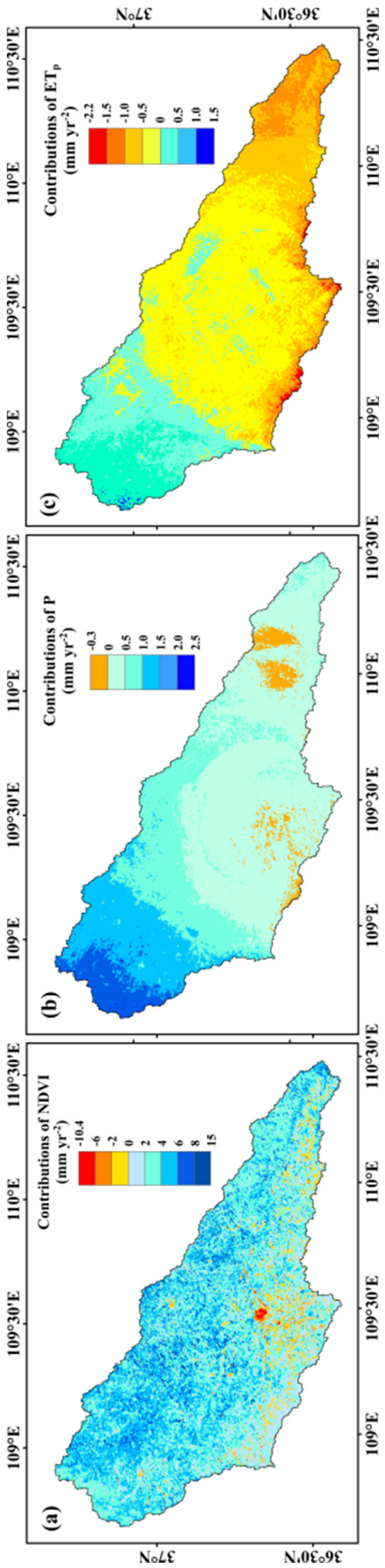

Fig. 13. Contributions of (a) vegetation greening (NDVI), (b) change in precipitation (P), and (c) change in ET_p to ET_a trend.

Averaged over the whole basin, the contributions of vegetation greening (V) and precipitation change (P) to the ET_a trend were positive, while ET_p (E) change showed a negative effect on ET_a trend (Fig. 14). From 2000 to 2016, the spatially averaged ET_a trend was 3.45 mm yr^{-2} (Net), of which changes in vegetation(V), precipitation (P) and ET_p(E) accounted for 93.0% (3.21 mm yr^{-2}), 18.1% (0.62 mm yr^{-2}) and − 7.4% (−0.26 mm yr^{-2}), respectively. Compared with direct effects, the two-way and three-way interactive effects were relatively low and accounted for a total of −3.7% (−0.13 mm yr^{-2}) of the ET_a trend. It is concluded that vegetation greening was the dominant driving factor for the long-term trend of ET_a from 2000 to 2016 in YRB.

De-trended variables were used to drive the model and the contribution of a single variable to the monthly ET_a trend was revealed. The contribution of a single variable to the ET_a trend was expressed by the differences simulated with the current and de-trended variable. As shown in Table 3, vegetation greening represented by NDVI was the primary driver for ET_a increases in summer months (May–Aug). However, in spring, precipitation had a more significant effect on the monthly ET_a change. As shown in Table 3, when precipitation was de-trended, the correlation coefficient of monthly ET_a with time turned from positive to negative in spring months. It is noteworthy that from Oct to Feb in the next year, the increase in NDVI had a weakly negative effect on monthly ET_a. This was mainly because that vegetation transpiration in autumn and winter is generally weak due to stomatal closure and leaf falling. Therefore, soil evaporation dominates the ET_a process in autumn and winter. However, the increase in vegetation cover reduced the radiation that reached the soil surface, thus the soil evaporation rate was depressed. Compared with NDVI and precipitation, other factors had relatively lower effects on the monthly ET_a trend.

4. Discussion

4.1. Modeling uncertainties

Although the remote-sensing based VIP model had good performance in predicting the annual ET_a over the YRB, it is worthwhile to explore the uncertainties of the results. First, the validation results showed a slight underestimation of the annual ET_a. This underestimation was partly attributed to the limitation that this model does not fully take into account of the impacts of the increase in soil and water retention induced by check-dams which were widely constructed on the Loess Plateau during the 1970s (Xu et al., 2004). By 2005, the density of check-dams on the Loess Plateau had reached to 1 check-dam per 5 km^2 (Xu et al., 2013a) but most of the check-dams are too small to be identified by MODIS sensor. Nonetheless, these impacts on the hydrological process may become weaker with time as check-dams were progressively filled with eroded material (Wang et al., 2016). Therefore, this limitation could not have significant influences on the final results because this study focused on the year-to-year and tendency changes of ET_a during the period of 2000–2016. Second, the sparse distribution of meteorological stations in this region affected the precisions of interpolation results and may be another cause of uncertainties. However, calculation of soil evaporation in this model is directly related to rainfall events rather than rainfall amount, thus the uncertainty associated with the high variability of precipitation is reduced (Mo et al., 2015).

This model avoided complicated algorithms and the resulting uncertainties by incorporating NDVI data into the predication of ET_a, because ET_a rates are strongly correlated with the product of vegetation index and temperature at mid-resolution pixels (Nagler et al., 2005). Here, we examined the effects of different parameterization schemes on the simulated annual ET_a by conducting sensitivity analysis of 5 key parameters (Fig. 15). Results showed that ET_a is most sensitive to changes in parameter $NDVI_{max}$, namely, 10% perturbation of $NDVI_{max}$ may result in up to 6.5% change of ET_a. The relative changes of ET_a induced by the perturbations of other parameters were all below 3% (absolute value). Therefore, the uncertainty range resulted from deviations of parameters was relatively small.

4.2. Change in ET and the driving factors

Although ET_p in YRB showed a slightly decreasing trend due to sunshine duration reduction and relative humidity increase, ET_a in YRB exhibited an increasing trend of 3.45 mm yr^{-1} during 2000–2016. Our results are generally in line with findings in other parts of the Loess Plateau. For instance, Wei et al. (2017) illustrated an increasing ET_a trend (1.90 mm yr^{-1}) in Northern Shaanxi Loess Plateau from 2000 to 2013; For the Loess Plateau as a whole, Gao et al. (2017) reported that with the increase of vegetation coverage, ET_a showed a significant increasing trend (1.34 mm yr^{-1}) during 1990 to 2014. Given that the YRB is one of the key areas of GFG project, the higher ET_a trend in YRB than that in other parts of the Loess Plateau is reasonable.

It is generally recognized that ET_p, vegetation condition, and soil water stress (mainly dominated by precipitation) are three main factors that control ET_a (Lettenmaier and Famiglietti, 2006). During the past decades, although air temperature showed a significant increasing trend, its positive effect on ET_a was offset by the negative effects of the declined wind speed and solar radiation, thus resulting in a decreasing ET_p trend over the Loess Plateau (She et al., 2017). The decrease in precipitation and ET_p might be the dominant factors for the decline in ET_a during 1980s and 1990s (Yang et al., 2016). However, based on the satellite-estimated ET_a datasets, Feng et al. (2016) found that GFG has caused ET_a to increase over the Loess Plateau, and the spatial pattern of ET_a trends coincides with that of the NDVI trends. These results indicated that the negative effects of climate change to ET_a on the Loess Plateau has been reversed by the increase of green leaf area, which would reduce land surface albedo and then leads to an increase of net radiation absorbed by the land surface.

4.3. Contributions of climate change and vegetation greening to water balance

During 2000 to 2016, vegetation greening was considered as the main cause of ET_a increase, accounting for 93.0% of the annual trend in ET_a. Meanwhile, climate change only contributed to 10.7% of the ET_a trend. Some other simulation studies in YRB also reached similar results, which confirmed that the revegetation played a dominant role in the reduction of streamflow and increase of ET_a in YRB (Qiu et al., 2017; Yang and Lu, 2018). Similar results can also be found in other GFG regions. For example, using four statistical runoff models, Li et al. (2016a) concluded that 85.2–90.3% of the runoff reduction in Wudinghe River basin, which is near YRB and also a key area of GFG project, may be attributed to Soil and Water Conservation measures. However, in Weihe River basin, where no significant vegetation greening was detected, climate change

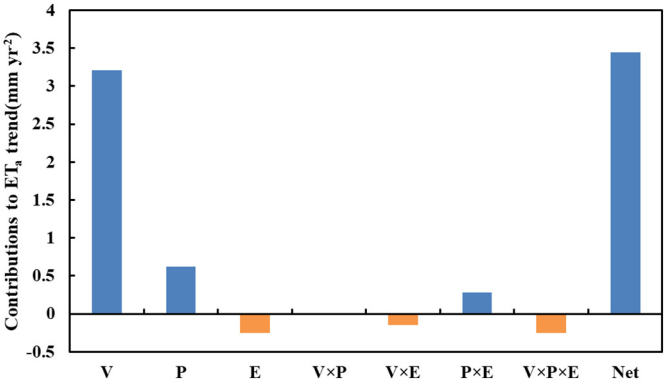

Fig. 14. Contributions of vegetation (V), precipitation (P), ET_p (E), and their two-way and three-way interactions to ET_a trend over the YRB.

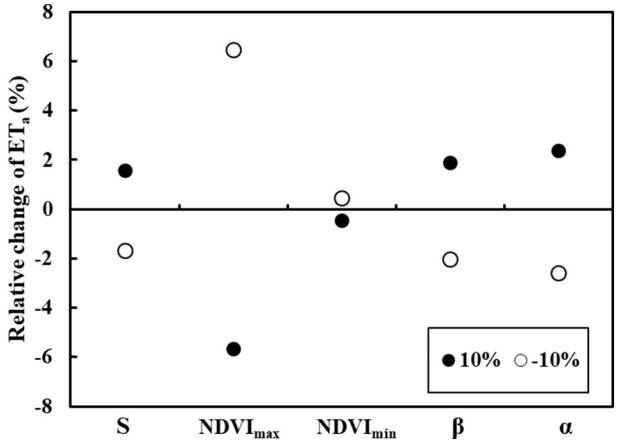

Fig. 15. Sensitivities of annual ET_a to soil-controlled exfiltration volume(S), parameters for calculation of f_c ($NDVI_{max}$,$NDVI_{max}$ and β) and extinction coefficient for net radiation (α).

was the main driving factor to the decline in runoff (Jiang et al., 2015). Although it is difficult to directly compare attribution results of different studies because analysis methods, reference periods, and hydrological variables used in these studies were different, it is clear that the contribution of GFG/LUCC to runoff reduction on the Loess Plateau was generally higher than that of climate change (Liang et al., 2015; Gao et al., 2016; Yang et al., 2015).

Furthermore, some studies reported that the relative contribution of LUCC to the water budget is gradually increasing (Tian et al., 2017; Li et al., 2016d). In Yellow River basin, the contribution rate of land surface change to runoff reduction in 2001–2010 is 78.4%, which is 10.2% higher than that in 1980–2000(Zhang et al., 2015b). This can be explained theoretically from the perspective of Budyko framework and elasticity of runoff. In the long term, partitioning of precipitation into runoff and ET_a is principally controlled by the dryness index ET_p/P and catchment landscape characteristics (described by the parameter n, and reforestation will lead to an increase of n) (Yang and Yang, 2011). With the increase of ET_p/P, both the absolute value of climate elasticity of runoff and that of catchment landscape elasticity of runoff increase, while the latter increases much faster (Xu et al., 2014; Yang and Yang, 2011). This indicates that the runoff is more sensitive to the change of catchment landscape under relatively dry climate conditions. Therefore, in terms of hydrological process, the role of catchment landscape is being more and more prominent.

4.4. Attribution of vegetation greening

The simulation experiments we used above did not completely differentiate the effects of climatic and anthropogenic factors on ET_a because vegetation greening is also a response of the terrestrial ecosystems to climate change. Here, we attributed the vegetation greening to climate change and GFG reforestation, which is denoted by afforestation area. Vegetation greening resulted from climate change can have an indirect effect on ET_a.

On the global or national scale, human-induced increasing CO_2 concentration is the dominant contributor to recent global trend in NDVI or LAI, followed by climate change, nitrogen deposition, and other factors (Zhao et al., 2018). In the study basin, the long-term trend of NDVI from 2000 to 2016 was 0.0094 yr^{-1}, which is about 30 times the global average NDVI increasing rate in the same period (Zhao et al., 2018). Therefore, we speculated that CO_2 fertilization was unlikely to be the dominant factor for vegetation coverage increase in YRB. On the other hand, temperature and precipitation, as key factors for plant growth, changed slightly during the same period (Table 2). Therefore, trend in climate can only have a marginal effect on vegetation greening in YRB. Correlation analysis showed that inter-annual variations of NDVI was significantly correlated with spring precipitation (SP) ($r = 0.61$, $p < 0.05$) and growing-season temperature (GT) ($r = -0.49$, $p < 0.1$), indicating that climate change may dominate the inter-annual variations of vegetation density. Based on the empirical relationship ($R^2 = 0.51$, $p = 0.01$) between NDVI, SP and GT, contributions of climatic variations to NDVI trend were estimated. As expected, climate change can only account for 9.3% of the NDVI trend.

There is no significant correlation between inter-annual variations of NDVI and afforestation area of current year. However, when the correlation analysis was performed on longer time steps, the close relationship between change of multi-year average NDVI and corresponding cumulative afforestation area was revealed ($r = 0.56$–0.83, $p < 0.05$). When the time step was extended to 5-year, the correlation coefficient reached the highest ($r = 0.83$, $p < 0.001$). This time delay of NDVI responding to afforestation indicated that afforestation in a year can have a vegetation greening effect that lasts for several years. Then, it is clear that vegetation greening was closely related with afforestation. In farmland, inter-annual change of NDVI was significantly correlated with that of grain yields ($r = 0.48$, $p < 0.1$), indicating that agricultural technology improvement exerted an explicit positive effect on NDVI increase in farmland. Therefore, it was affirmed that the long-term trend of NDVI in the YRB was mainly driven by GFG revegetation.

4.5. Implications

Afforestation can improve ecosystem productivity, but may change regional water budget, resulting in a potential water demand conflicting between natural ecosystem and socio-economic system (Tang et al., 2018). Changes in vegetation pattern have a direct effect on water resources by altering the partitioning of precipitation into runoff and ET_a (Donohue et al., 2007). As shown in Fig. 16, with the continuous increase of NDVI after 2000, the runoff coefficient in Ganguyi sub-basin continued to decrease with an average speed of 0.0008 yr^{-1}. The average runoff coefficient in 2000–2016 is 0.02 lower than that in 1980–1999. Similar results can be found in other parts of the Loess Plateau (Li et al., 2016b; Gao et al., 2016). Liu et al. (2014) found that when vegetation coverage of grass and forest increased by 1% since 1970s, the runoff coefficient in semi-humid and semi-dry regions of the Loess Plateau could decreased by 0.0009 and 0.0051, respectively.

The response of soil water to afforestation is somewhat complicated. Increase of vegetation cover can decrease the net precipitation by increasing the interception amounts in small rainfall events; however, it can also increase the infiltration amounts in heavy rainfall events by increasing the surface roughness and soil water storage capacity. As summer rainfall on the Loess Plateau mainly occurs in the form of heavy rain, we can speculate that there would be an increase in soil moisture.

Table 2
Inter-annual trends of monthly climatic variables from 2000 to 2016 in YRB.

Climatic variables	Jan	Feb	Mar	Apr	May	Jun	Jul	Aug	Sep	Oct	Nov	Dec	Annual
T(°C yr^{-1})	−0.010	−0.098	0.015	0.032	−0.087	−0.051	−0.054	0.030	0.001	0.070	0.068	0.029	−0.004
P(mm yr^{-1})	−0.34	0.27	0.25	1.02	1.15	−1.54	3.29	−0.45	0.06	−0.59	0.92	−0.06	3.98
RH(% yr^{-1})	−0.911*	−0.004	0.184	0.368	0.260	0.074	0.185	−0.123	0.153	−0.171	0.286	−0.133	0.011
U(m s^{-1} yr^{-1})	0.011	0.016*	0.000	−0.006	0.007	0.010	0.003	0.011*	0.009	0.013*	0.012*	0.012	0.009*
Sun(h yr^{-1})	1.2	−1.2	−1.4	0.5	−1.5	−0.8	−2.0	0.3	−1.1	0.2	−2.8	0.5	−8.1

Significance level:*($p < 0.05$) **($p < 0.01$).

Table 3
Monthly Pearson correlation coefficients of ET_a trends (r_ALL: all variables are not de-trended; r_T, r_U, r_S, r_P and r_NDVI: air temperature, wind speed, sunshine duration, precipitation, and NDVI are de-trended respectively).

	Jan	Feb	Mar	Apr	May	Jun	Jul	Aug	Sep	Oct	Nov	Dec
r_All	−0.50	0.14	0.02	0.21	0.58	0.51	0.65	0.64	0.24	−0.20	0.08	0.05
r_T	−0.51	0.18	0.00	0.17	0.68	0.56	0.67	0.59	0.22	−0.40	0.04	0.03
r_U	−0.50	0.13	0.02	0.22	0.57	0.49	0.65	0.64	0.24	−0.23	0.06	0.03
r_S	−0.50	0.14	0.02	0.21	0.61	0.54	0.73	0.62	0.33	−0.20	0.09	0.06
r_P	0.02	0.20	−0.12	−0.10	0.47	0.61	0.37	0.66	0.26	−0.02	−0.08	0.12
r_NDVI	−0.45	0.19	0.04	0.15	0.36	−0.23	0.02	0.17	0.08	−0.02	0.24	0.16

However, many studies have demonstrated widespread soil desiccation over the Loess Plateau (Jian et al., 2015; Jia et al., 2017; Ren et al., 2018; Jia and Shao, 2014), suggesting that the increased infiltration amounts have been overweighed by the extra water consumption of new plantation and higher vegetation coverage. To maintain both the socio-economic and ecological sustainability, a threshold of vegetation cover on the Loess Plateau should be considered in future reforestation (Feng et al., 2016; Zhang et al., 2018), because vegetation restoration is largely controlled by soil water availability in arid and semi-arid regions (Porporato et al., 2002). Therefore, we recommend a more rational design of vegetation species and planting densities for future implementation of GFG program.

5. Conclusion

In this paper, the spatial-temporal pattern of ET_a was estimated from 2000 to 2016 over the YRB using the remote-sensing based VIP model. Dominant driving factor that controlled inter-annual changes of ET_a for each pixel was identified through partial correlation analysis. Contributions of climate change and vegetation greening to ET_a trend were quantitatively differentiated after 8 model experiments were conducted.

Over the whole basin, averaged annual ET_a showed a significant increasing trend from 2000 to 2016 with a trend of 3.45 mm yr^{-1}, and the significant increase mainly occurred in summer months (May-Aug). On an annual scale, partial correlation analysis showed that the inter-annual change of ET_a was driven by NDVI in 56% area of the YRB. Model simulation experiments indicated that contributions of NDVI, precipitation, and ET_p to ET_a trend were 93%, 18.1%, and −7.4%, respectively. On a monthly scale, NDVI was the dominant driving factor for ET_a trend in summer months. However, in spring, precipitation had a more significant effect on ET_a trend. In autumn and winter (Oct–Feb in the next year), increase in NDVI reduced energy available for soil evaporation, thus exerting a slightly negative effects on ET_a. It is concluded that vegetation greening, which was strongly related to the GFG reforestation, was the main driver to the long-term tendency of water consumption in the YRB. To maintain a sustainable eco-hydrological environment on the Loess Plateau, a more rational design of vegetation species and planting densities should be determined to guide the future GFG reforestation.

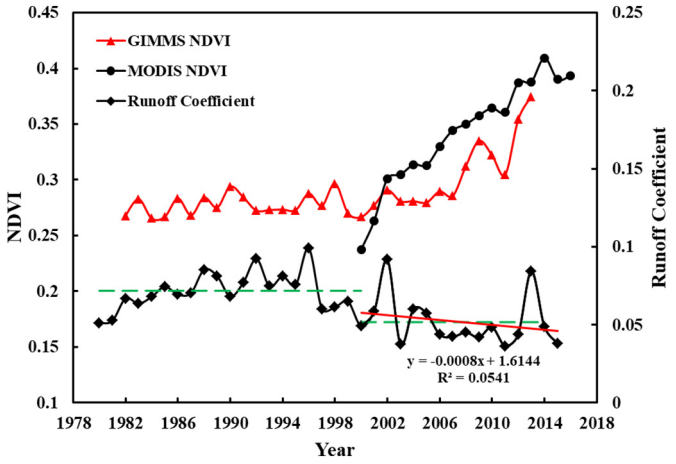

Fig. 16. Time series of runoff coefficient and GIMMS/MODIS NDVI from 1980 to 2016 in Ganguyi sub-basin of YRB.

Acknowledgement

This study was financially supported by the National Natural Science Foundation of China (No. 41790424). We thank the Editor and anonymous reviewers for their constructive comments, which improved the quality of this paper.

Appendix A. Model description

The remote-sensing based VIP model was designed to simulate the exchanges of energy and water between land surface and atmosphere (Mo et al., 2015). In this model, actual ET (ET_a) is composed of vegetation transpiration (E_c), soil evaporation (E_s), and canopy interception evaporation (E_i). Vegetation transpiration is estimated based on potential transpiration (E_{cp}), mediated by the minimum stomatal resistance and the environmental stresses, and expressed as follows:

$$E_c = E_{cp} f_w f_t \tag{1}$$

where f_w and f_t indicate stress functions of atmospheric water vapor pressure deficit and air temperature, respectively, and they are calculated using algorithms proposed by Mu et al. (2007) and Zhang et al. (2010). E_{cp} is calculated using the Penman-Monteith equation as follows:

$$E_{cp} = \frac{1}{\lambda}\left(\Delta R_{nc} + f_c \rho c_p D / r_a\right) / (\Delta + \gamma\eta) \tag{2}$$

where R_{nc} refers to the net radiation absorbed by the canopy; f_c denotes the fractional vegetation cover; Δ represent the slope of the saturated vapor pressure curve versus air temperature; η indicate the ratio of the minimum stomatal resistance of a natural plant functional type to that of the reference crop; λ is the latent heat of vaporization of water; r_a is the aerodynamic resistance between the canopy and the reference height; γ, ρ, c_p and D represent the psychrometric constant, air density specific heat capacity of air and vapor-pressure deficit, respectively.

Evaporation from canopy interception (E_i) equals to the potential evaporation over its wetted surface; Soil evaporation (E_s) is restricted by surface potential evaporation (E_{sp}) and soil moisture exfiltration (E_{ex}), which decreases as surface soil moisture depletes, namely,

$$E_s = \min\left(E_{sp}, E_{ex}\right) \tag{3}$$

$$E_{sp} = \frac{1}{\lambda}\left[\Delta(R_{ns} - G) + (1 - f_c)\rho c_p D / r_{as}\right] / (\Delta + \gamma) \tag{4}$$

$$E_{ex} = S\left(t^{0.5} - (t-1)^{0.5}\right) \tag{5}$$

where R_{ns} is the net radiation absorbed by the soil surface; G is the soil heat flux; r_{as} is the aerodynamic resistance between reference

height and soil surface; S is the soil-controlled exfiltration volume and usually falls by 3–5 mm $d^{-1.5}$(in this study a value of 3.5 mm $d^{-1.5}$ is set); t is the time (days) elapsed since the day following rainfall.

Net radiation at the top of canopy (R_n) is retrieved from observed sunshine duration with empirical relationships proposed by Allen et al. (1998). R_n is further partitioned into energy for soil and canopy (R_{ns} for the soil, and R_{nc} for the canopy), using a layer approach based on Beer's law:

$$R_{ns} = R_n e^{-\alpha LAI} \tag{6}$$

$$R_{nc} = R_n\left(1-e^{-\alpha LAI}\right) \tag{7}$$

where α is the extinction coefficient for net radiation; LAI is the leaf area index which is retrieved from vegetation fraction with empirical relationship. Vegetation fraction (f_c) is estimated using empirical formula based on remote sensing vegetation index:

$$f_c = 1-\left(\frac{\mathrm{NDVI}_{\max}-\mathrm{NDVI}}{\mathrm{NDVI}_{\max}-\mathrm{NDVI}_{\min}}\right)^{\beta} \tag{7}$$

where β is an empirical constant ranging from 0.6 to 1.2 and $\beta = 0.9$ is used in this study; $\mathrm{NDVI}_{\max}$ and $\mathrm{NDVI}_{\min}$ represent NDVI values for conditions of full vegetation cover and bare soil, respectively.

The dynamics of soil moisture (SM) is introduced through a three-layer scheme, in which the first layer works as a significant source of soil evaporation, the second as the source of root uptake for canopy transpiration and the third layer as the drainage layer. SM Modeling in different layers is based on water-balance equations which incorporate E_s and E_c as the primary water budget components, namely:

$$\frac{\partial\theta_1}{\partial t} = \frac{1}{L_1}\left(P_n-Q_{1,2}-E_s\right) \tag{8}$$

$$\frac{\partial\theta_2}{\partial t} = \frac{1}{L_2}\left(Q_{1,2}-Q_{2,3}-E_c\right) \tag{9}$$

$$\frac{\partial\theta_3}{\partial t} = \frac{1}{L_3}\left(Q_{2,3}-Q_3\right) \tag{10}$$

where θ_i ($i = 1,2,3$) is the soil moisture in the soil layer i with thickness L_i, and is set to 2, 98 and 60 cm for layer 1, 2 and 3, respectively; P_n is the net precipitation; $Q_{i,\,i+1}$ ($i = 1,2$) is the flow between layer i and layer $i + 1$ and estimated following the method of Sellers et al. (1986); Q_3 is the gravitational drainage from the third layer and is calculated following Darcy's law. Soil hydraulic parameters are estimated using the scheme of Clapp and Hornberger (1978).

References

Allen, R.G., Pereira, L.S., Raes, D., Smith, M., 1998. Crop Evapotranspiration: Guidelines for Computing Crop Water Requirements, FAO Irrigation and Drainage Paper No 56. Food and Agriculture Organization, United Nations, Rome, Italy.

Bai, P., Liu, X., Zhang, Y., Liu, C., 2018a. Incorporating vegetation dynamics noticeably improved performance of hydrological model under vegetation greening. Sci. Total Environ. 643, 610–622.

Bai, P., Liu, X.M., Liu, C.M., 2018b. Improving hydrological simulations by incorporating GRACE data for model calibration. J. Hydrol. 557, 291–304.

Budyko, M.I., 1974. Climate and Life, Transl. from Russian by D. H. Miller. Academic Press, San Diego, CA.

Cao, Z., Li, Y., Liu, Y., Chen, Y., Wang, Y., 2018. When and where did the Loess Plateau turn "green"? Analysis of the tendency and breakpoints of the normalized difference vegetation index. Land Degradation & Development 29, 162–175.

Chen, J., Jonsson, P., Tamura, M., Gu, Z.H., Matsushita, B., Eklundh, L., 2004. A simple method for reconstructing a high quality NDVI time-series data set based on the Savitzky–Golay filter. Remote Sens. Environ. 91, 332–344.

Chen, Y.P., Wang, K.B., Lin, Y.S., Shi, W.Y., Song, Y., He, X.H., 2015. Balancing green and grain trade. Nat. Geosci. 8, 739–741.

Chen, X., Mo, X., Hu, S., Liu, S., 2017. Contributions of climate change and human activities to ET and GPP trends over North China plain from 2000 to 2014. J. Geogr. Sci. 27, 661–680.

Clapp, R.B., Hornberger, G.M., 1978. Empirical equations for some soil hydraulic-properties. Water Resour. Res. 14, 601–604.

Donohue, R.J., Roderick, M.L., McVicar, T.R., 2007. On the importance of including vegetation dynamics in Budyko's hydrological model. Hydrol. Earth Syst. Sci. 11, 983–995.

Douville, H., Ribes, A., Decharme, B., Alkama, R., Sheffield, J., 2013. Anthropogenic influence on multidecadal changes in reconstructed global evapotranspiration. Nat. Clim. Chang. 3, 59–62.

Feng, X., Fu, B., Lu, N., Zeng, Y., Wu, B., 2013. How ecological restoration alters ecosystem services: an analysis of carbon sequestration in China's Loess Plateau. Sci. Rep. 3, 2846.

Feng, X., Fu, B., Piao, S., Wang, S., Ciais, P., Zeng, Z., Lü, Y., Zeng, Y., Li, Y., Jiang, X., Wu, B., 2016. Revegetation in China's Loess Plateau is approaching sustainable water resource limits. Nat. Clim. Chang. 6, 1019–1022.

Fisher, J.B., Whittaker, R.J., Malhi, Y., 2011. ET come home: potential evapotranspiration in geographical ecology. Glob. Ecol. Biogeogr. 20, 1–18.

Gao, G., Fu, B., Wang, S., Liang, W., Jiang, X., 2016. Determining the hydrological responses to climate variability and land use/cover change in the Loess Plateau with the Budyko framework. Sci. Total Environ. 557-558, 331–342.

Gao, X., Sun, M., Zhao, Q., Wu, P., Zhao, X., Pan, W., Wang, Y., 2017. Actual ET modelling based on the Budyko framework and the sustainability of vegetation water use in the Loess Plateau. Sci. Total Environ. 579, 1550–1559.

Gong, T., Lei, H., Yang, D., Jiao, Y., Yang, H., 2017. Monitoring the variations of evapotranspiration due to land use/cover change in a semiarid shrubland. Hydrol. Earth Syst. Sci. 21, 863–877.

Hou, Y., Lü, Y., Chen, W., Fu, B., 2017. Temporal variation and spatial scale dependency of ecosystem service interactions: a case study on the central Loess Plateau of China. Landsc. Ecol. 32, 1201–1217.

Huang, Z., Yang, H., Yang, D., 2016. Dominant climatic factors driving annual runoff changes at the catchment scale across China. Hydrol. Earth Syst. Sci. 20, 2573–2587.

Jia, Y.-H., Shao, M.-A., 2014. Dynamics of deep soil moisture in response to vegetational restoration on the Loess Plateau of China. J. Hydrol. 519, 523–531.

Jia, X., Shao, M.a., Zhu, Y., Luo, Y., 2017. Soil moisture decline due to afforestation across the Loess Plateau, China. J. Hydrol. 546, 113–122.

Jian, S., Zhao, C., Fang, S., Yu, K., 2015. Effects of different vegetation restoration on soil water storage and water balance in the Chinese Loess Plateau. Agric. For. Meteorol. 206, 85–96.

Jiang, C., Xiong, L.H., Wang, D.B., Liu, P., Guo, S.L., Xu, C.Y., 2015. Separating the impacts of climate change and human activities on runoff using the Budyko-type equations with time-varying parameters. J. Hydrol. 522, 326–338.

Jiao, Q., Li, R., Wang, F., Mu, X., Li, P., An, C., 2016. Impacts of re-vegetation on surface soil moisture over the Chinese Loess Plateau based on remote sensing datasets. Remote Sens. 8.

Jin, Z., Liang, W., Yang, Y., Zhang, W., Yan, J., Chen, X., Li, S., Mo, X., 2017. Separating vegetation greening and climate change controls on evapotranspiration trend over the Loess Plateau. Sci. Rep. 7, 8191.

Landerer, F.W., Swenson, S.C., 2012. Accuracy of scaled GRACE terrestrial water storage estimates. Water Resour. Res. 48.

Lettenmaier, D.P., Famiglietti, J.S., 2006. Hydrology - water from on high. Nature 444, 562–563.

Li, Z., Liu, W.-z., Zhang, X.-c., Zheng, F.-l., 2009. Impacts of land use change and climate variability on hydrology in an agricultural catchment on the Loess Plateau of China. J. Hydrol. 377, 35–42.

Li, S., Yang, S., Liu, X., Liu, Y., Shi, M., 2015. NDVI-based analysis on the influence of climate change and human activities on vegetation restoration in the Shaanxi-Gansu-Ningxia Region, Central China. Remote Sensing 7, 11163–11182.

Li, B., Liang, Z., Zhang, J., Wang, G., Zhao, W., Zhang, H., Wang, J., Hu, Y., 2016a. Attribution analysis of runoff decline in a semiarid region of the Loess Plateau, China. Theor. Appl. Climatol. 131, 845–855.

Li, S., Liang, W., Fu, B., Lu, Y., Fu, S., Wang, S., Su, H., 2016b. Vegetation changes in recent large-scale ecological restoration projects and subsequent impact on water resources in China's Loess Plateau. Sci Total Environ 569-570, 1032–1039.

Li, S., Liang, W., Zhang, W., Liu, Q., 2016c. Response of soil moisture to hydro-meteorological variables under different precipitation gradients in the Yellow River Basin. Water Resour. Manag. 30, 1867–1884.

Li, Y., Liu, C., Zhang, D., Liang, K., Li, X., Dong, G., 2016d. Reduced Runoff Due to Anthropogenic Intervention in the Loess Plateau, China. Water 8.

Li, G., Zhang, F., Jing, Y., Liu, Y., Sun, G., 2017a. Response of evapotranspiration to changes in land use and land cover and climate in China during 2001–2013. Sci. Total Environ. 596-597, 256–265.

Li, J., Peng, S., Li, Z., 2017b. Detecting and attributing vegetation changes on China's Loess Plateau. Agric. For. Meteorol. 247, 260–270.

Liang, W., Bai, D., Wang, F., Fu, B., Yan, J., Wang, S., Yang, Y., Long, D., Feng, M., 2015. Quantifying the impacts of climate change and ecological restoration on streamflow changes based on a Budyko hydrological model in China's Loess Plateau. Water Resour. Res. 51, 6500–6519.

Liu, S.M., Xu, Z.W., Wang, W.Z., Jia, Z.Z., Zhu, M.J., Bai, J., Wang, J.M., 2011. A comparison of eddy-covariance and large aperture scintillometer measurements with respect to the energy balance closure problem. Hydrol. Earth Syst. Sci. 15, 1291–1306.

Liu, X., Liu, C., Yang, S., 2014. Influences of shrubs-herbs-arbor vegetation coverage on the runoff based on the remote sensing data in Loess Plateau. Acta Geograph. Sin. 69, 1595–1603.

Liu, Y., Xiao, J., Ju, W., Xu, K., Zhou, Y., Zhao, Y., 2016. Recent trends in vegetation greenness in China significantly altered annual evapotranspiration and water yield. Environ. Res. Lett. 11.

Mo, X.G., Liu, S.X., 2001. Simulating evapotranspiration and photosynthesis of winter wheat over the growing season. Agric. For. Meteorol. 109, 203–222.

Mo, X., Liu, S., Lin, Z., Zhao, W., 2004. Simulating temporal and spatial variation of evapotranspiration over the Lushi basin. J. Hydrol. 285, 125–142.
Mo, X., Liu, S., Lin, Z., Xu, Y., Xiang, Y., McVicar, T.R., 2005. Prediction of crop yield, water consumption and water use efficiency with a SVAT-crop growth model using remotely sensed data on the North China plain. Ecol. Model. 183, 301–322.
Mo, X., Liu, S., Lin, Z., Wang, S., Hu, S., 2015. Trends in land surface evapotranspiration across China with remotely sensed NDVI and climatological data for 1981–2010. Hydrol. Sci. J. 60, 2163–2177.
Mo, X., Chen, X., Hu, S., Liu, S., Xia, J., 2017. Attributing regional trends of evapotranspiration and gross primary productivity with remote sensing: a case study in the North China plain. Hydrol. Earth Syst. Sci. 21, 295–310.
Mu, Q., Heinsch, F.A., Zhao, M., Running, S.W., 2007. Development of a global evapotranspiration algorithm based on MODIS and global meteorology data. Remote Sens. Environ. 111, 519–536.
Nagler, P.L., Cleverly, J., Glenn, E., Lampkin, D., Huete, A., Wan, Z.M., 2005. Predicting riparian evapotranspiration from MODIS vegetation indices and meteorological data. Remote Sens. Environ. 94, 17–30.
Nalder, I.A., Wein, R.W., 1998. Spatial interpolation of climatic Normals: test of a new method in the Canadian boreal forest. Agric. For. Meteorol. 92, 211–225.
Ning, T., Li, Z., Liu, W., 2017. Vegetation dynamics and climate seasonality jointly control the interannual catchment water balance in the Loess Plateau under the Budyko framework. Hydrol. Earth Syst. Sci. 21, 1515–1526.
Patle, G.T., Singh, D.K., 2015. Sensitivity of annual and seasonal reference crop evapotranspiration to principal climatic variables. Journal of Earth System Science 124, 819–828.
Pei, T., Wu, X., Li, X., Zhang, Y., Shi, F., Ma, Y., Wang, P., Zhang, C., 2017. Seasonal divergence in the sensitivity of evapotranspiration to climate and vegetation growth in the Yellow River Basin, China. Journal of Geophysical Research: Biogeosciences 122, 103–118.
Porporato, A., D'Odorico, P., Laio, F., Ridolfi, L., Rodriguez-Iturbe, I., 2002. Ecohydrology of water-controlled ecosystems. Adv. Water Resour. 25, 1335–1348.
Qiu, L., Wu, Y., Wang, L., Lei, X., Liao, W., Hui, Y., Meng, X., 2017. Spatiotemporal response of the water cycle to land use conversions in a typical hilly–gully basin on the Loess Plateau, China. Hydrology and Earth System Sciences 21, 6485–6499.
Ren, Z., Li, Z., Liu, X., Li, P., Cheng, S., Xu, G., 2018. Comparing watershed afforestation and natural revegetation impacts on soil moisture in the semiarid Loess Plateau of China. Sci. Rep. 8, 2972.
Roderick, M.L., Farquhar, G.D., 2011. A simple framework for relating variations in runoff to variations in climatic conditions and catchment properties. Water Resour. Res. 47.
Sellers, P.J., Mintz, Y., Sud, Y.C., Dalcher, A., 1986. A simple biosphere model (sib) for use within general-circulation models. J. Atmos. Sci. 43, 505–531.
She, D.X., Xia, J., Zhang, Y.Y., 2017. Changes in reference evapotranspiration and its driving factors in the middle reaches of Yellow River Basin, China. Science of the Total Environment 607, 1151–1162.
Shen, M., Piao, S., Jeong, S.J., Zhou, L., Zeng, Z., Ciais, P., Chen, D., Huang, M., Jin, C.S., Li, L.Z., Li, Y., Myneni, R.B., Yang, K., Zhang, G., Zhang, Y., Yao, T., 2015. Evaporative cooling over the Tibetan Plateau induced by vegetation growth. Proc. Natl. Acad. Sci. U. S. A. 112, 9299–9304.
Stein, U., Alpert, P., 1993. Factor separation in numerical simulations. J. Atmos. Sci. 50, 2107–2115.
Sun, G., Zhou, G., Zhang, Z., Wei, X., McNulty, S.G., Vose, J.M., 2006. Potential water yield reduction due to forestation across China. J. Hydrol. 328, 548–558.
Sun, G., Zuo, C.Q., Liu, S.Y., Liu, M.L., McNulty, S.G., Vose, J.M., 2008. Watershed evapotranspiration increased due to changes in vegetation composition and structure under a subtropical climate. J. Am. Water Resour. Assoc. 44, 1164–1175.
Tang, L.-L., Cai, X.-B., Gong, W.-S., Lu, J.-Z., Chen, X.-L., Lei, Q., Yu, G.-L., 2018. Increased vegetation greenness aggravates water conflicts during lasting and intensifying drought in the Poyang Lake watershed, China. Forests 9.
Tapley, B.D., Bettadpur, S., Ries, J.C., Thompson, P.F., Watkins, M.M., 2004. GRACE measurements of mass variability in the Earth system. Science 305, 503–505.
Tian, F., Lü, Y.H., Fu, B.J., Zhang, L., Zang, C.f., Yang, Y.H., Qiu, G.Y., 2017. Challenge of vegetation greening on water resources sustainability: insights from a modeling-based analysis in Northwest China. Hydrol. Process. 31, 1469–1478.
Wang, D.B., Hejazi, M., 2011. Quantifying the relative contribution of the climate and direct human impacts on mean annual streamflow in the contiguous United States. Water Resour. Res. 47.
Wang, Y., Yu, P., Xiong, W., Shen, Z., Guo, M., Shi, Z., Du, A., Wang, L., 2008. Water-yield reduction after afforestation and related processes in the semiarid Liupan Mountains, northwest China1. JAWRA Journal of the American Water Resources Association 44, 1086–1097.
Wang, F., Hessel, R., Mu, X., Maroulis, J., Zhao, G., Geissen, V., Ritsema, C., 2015. Distinguishing the impacts of human activities and climate variability on runoff and sediment load change based on paired periods with similar weather conditions: a case in the Yan River, China. Journal of Hydrology 527, 884–893.
Wang, S.A., Fu, B.J., Piao, S.L., Lu, Y.H., Ciais, P., Feng, X.M., Wang, Y.F., 2016. Reduced sediment transport in the Yellow River due to anthropogenic changes. Nature Geoscience 9 (38-+).
Wang, H., Liu, G., Li, Z., Ye, X., Fu, B., Lü, Y., 2017. Analysis of the driving forces in vegetation variation in the grain for green program region, China. Sustainability 9.
Wei, H., Fan, W., Ding, Z., Weng, B., Xing, K., Wang, X., Lu, N., Ulgiati, S., Dong, X., 2017. Ecosystem services and ecological restoration in the Northern Shaanxi Loess Plateau, China, in relation to climate fluctuation and Investments in Natural Capital. Sustainability 9.
Wohlfart, C., Liu, G., Huang, C., Kuenzer, C., 2016. A River Basin over the course of time: multi-temporal analyses of land surface dynamics in the Yellow River Basin (China) based on medium resolution remote sensing data. Remote Sens. 8.
Xie, X., Liang, S., Yao, Y., Jia, K., Meng, S., Li, J., 2015. Detection and attribution of changes in hydrological cycle over the three-north region of China: climate change versus afforestation effect. Agric. For. Meteorol. 203, 74–87.
Xu, X.Z., Zhang, H.W., Zhang, O.Y., 2004. Development of check-dam systems in gullies on the Loess Plateau, China. Environmental Science & Policy 7, 79–86.
Xu, Y.D., Fu, B.J., He, C.S., 2013a. Assessing the hydrological effect of the check dams in the Loess Plateau, China, by model simulations. Hydrol. Earth Syst. Sci. 17, 2185–2193.
Xu, Z.W., Liu, S.M., Li, X., Shi, S.J., Wang, J.M., Zhu, Z.L., Xu, T.R., Wang, W.Z., Ma, M.G., 2013b. Intercomparison of surface energy flux measurement systems used during the HiWATER-MUSOEXE. J. Geophys. Res.-Atmos. 118, 13140–13157.
Xu, X., Yang, D., Yang, H., Lei, H., 2014. Attribution analysis based on the Budyko hypothesis for detecting the dominant cause of runoff decline in Haihe basin. J. Hydrol. 510, 530–540.
Yang, K.J., Lu, C.H., 2018. Evaluation of land-use change effects on runoff and soil erosion of a hilly basin the Yanhe River in the Chinese Loess Plateau. Land Degrad. Dev. 29, 1211–1221.
Yang, H.B., Yang, D.W., 2011. Derivation of climate elasticity of runoff to assess the effects of climate change on annual runoff. Water Resour. Res. 47.
Yang, D., Zhang, S., Xu, X., 2015. Attribution analysis for runoff decline in Yellow River Basin during past fifty years based on Budyko hypothesis. Scientia Sinica Technologica 45, 1024–1034.
Yang, Z., Zhang, Q., Hao, X., 2016. Evapotranspiration trend and its relationship with precipitation over the Loess Plateau during the last three decades. Adv. Meteorol. 2016, 1–10.
Yao, Y., Liang, S., Zhao, S., Zhang, Y., Qin, Q., Cheng, J., Jia, K., Xie, X., Zhang, N., Liu, M., 2014. Validation and application of the modified satellite-based Priestley-Taylor algorithm for mapping terrestrial evapotranspiration. Remote Sens. 6, 880–904.
Yin, J., He, F., Xiong, Y.J., Qiu, G.Y., 2017. Effects of land use/land cover and climate changes on surface runoff in a semi-humid and semi-arid transition zone in Northwest China. Hydrol. Earth Syst. Sci. 21, 183–196.
Zhang, K., Kimball, J.S., Nemani, R.R., Running, S.W., 2010. A continuous satellite-derived global record of land surface evapotranspiration from 1983 to 2006. Water Resour. Res. 46.
Zhang, K., Kimball, J.S., Nemani, R.R., Running, S.W., Hong, Y., Gourley, J.J., Yu, Z., 2015a. Vegetation greening and climate change promote multidecadal rises of global land evapotranspiration. Sci Rep 5, 15956.
Zhang, S., Yang, D., Yang, H., Lei, H., 2015b. Analysis of the dominant causes for runoff reduction in five major basins over China during 1960–2010. Adv. Water Sci. 26, 605–613.
Zhang, K., Kimball, J.S., Running, S.W., 2016. A review of remote sensing based actual evapotranspiration estimation. Wiley Interdiscip. Rev. Water 3, 834–853.
Zhang, S., Yang, D., Yang, Y., Piao, S., Yang, H., Lei, H., Fu, B., 2018. Excessive afforestation and soil drying on China's Loess Plateau. Journal of Geophysical Research: Biogeosciences 123, 923–935.
Zhao, L., Dai, A., Dong, B., 2018. Changes in global vegetation activity and its driving factors during 1982–2013. Agric. For. Meteorol. 249, 198–209.